PROCEEDINGS OF SCIENCE

The origin of the very-high-energy radiation of Centaurus A

Cainã de Oliveira,[a,*] **James H. Matthews**[b] **and Vitor de Souza**[a]

[a] *São Carlos Institute of Physics, University of São Paulo, IFSC – USP*
13566-590, São Carlos, SP, Brazil.

[b] *Department of Physics, Astrophysics, University of Oxford*
Denys Wilkinson Building, Keble Road, Oxford OX1 3RH, UK

E-mail: olivcaina@gmail.com, caina.oliveira@usp.br

As the closest known active galactic nucleus, Centaurus A provides a rich environment for astrophysical exploration, being detected from radio to gamma rays. Recently, very-high-energy gamma rays have been measured by the HESS observatory. The signal is associated with the jet, revealing the presence of relativistic electrons. However, the underlying acceleration mechanism remains uncertain. Several works have proposed that jet substructures, known as knots, may act as efficient particle accelerators. In this work, we model the particle acceleration in the knots, assuming they originate from the interactions between the jet and powerful stellar winds. The knots are modeled using relativistic hydrodynamics simulations using the PLUTO code. It is assumed that the shock injects relativistic electrons whose maximum energy depends on the radiation fields of the galaxy. The spectral index is found based on the radio and X-ray observed data, assuming a synchrotron origin. Inverse Compton scattering of the same electron population produces the very-high-energy γ rays in this model. Our findings suggest that electrons accelerated at the knots are responsible for the γ-ray spectrum detected in the very-high-energy band. The possibility of knots as ultra-high-energy cosmic ray accelerators is also explored.

39th International Cosmic Ray Conference (ICRC2025)
15–24 July 2025
Geneva, Switzerland

ICRC 2025
The Astroparticle Physics Conference
Geneva July 15-24, 2025

*Speaker

PoS(ICRC2025)623

1. Introduction

Centaurus A (Cen A) is the closest radio galaxy, at a distance 3.8 Mpc [1]. It is ejecting collimated jets, which have been resolved in radio and X-ray wavelengths [2, 3]. In addition, Cen A is an important source of high-energy radiation. Recently, the HESS Collaboration reported the detection of an extended emission of very-high-energy γ radiation along the jet of Cen A [4]. The γ-ray signal favors a synchrotron interpretation for the X-ray emission detected along the jet, and suggests the existence of an efficient particle acceleration mechanism acting far away from the central black hole. However, this underlying acceleration mechanism remains uncertain.

The jet of Cen A presents substructures known as knots. There are both stationary and moving knots detected in radio and X-ray wavelengths [3, 5]. The majority of the knots can be explained by collisions of the jet with obstacles, generating a local shock complex. Stationary shocks can be produced by collisions with the stellar wind (SW) from high mass-loss rate stars, such as AGB, O/B, and/or Wolf-Rayet (WR) stars [2, 3, 6]. Collisions between the jet and stellar winds produce shock waves and regions of magnetic field amplification suitable for long-lived particle acceleration [7]. Accelerated electrons will produce non-thermal radiation from synchrotron and Inverse Compton losses. The last have been proposed to generate γ radiation, potentially explaining the γ rays excess observed from Cen A [8, 9].

More than 40 knots have been detected by *Chandra* along the jet of Cen A [3, 5]. The brightest X-ray knots, at 1 keV, are distributed closer to the core, in the AX and BX groups [3]. In this work, we build a detailed model for the brightest knots AX1A, AX1C, AX2, and BX2 and predict the acceleration of electrons on them. After testing the model, we extended the analysis for other stationary knots and evaluated the expected γ-ray signal. For more details see the main publication ref. [10].

2. Modelling the knots

Our model for the knots is based on the following steps: obtain the hydrodynamic profile for the jet/SW interaction; estimate the electron population in the simulation grid; and predict the non-thermal emission from the electrons. These steps are detailed below.

2.1 Hydrodynamic profile

The fluid equations for the jet/SW collision were solved using the Relativistic Hydrodynamics (RHD) module from `PLUTO` code [11]. The simulation was performed in a 2D setup, assuming cylindrical symmetry with a grid of 300×800 cells, considering the interval $r_{\rm sim} = [0, 1.5]$, $z_{\rm sim} = [0, 4.0]$. Computation units are converted to physical units considering the jet radius (R_j) at the distance from the respective knot from the core ($z_{\rm knot}$). The plasma is assumed to follow the Taub-Matthews equation of state.

The initial velocity, pressure, and density of the plasma in the jet were obtained from data available for Cen A. The jet speed was taken equal to $v_j = 0.6c$ [2] along the jet direction ($\hat{z}$). The jet is assumed to be in mechanical equilibrium with the external medium. The external pressure was estimated using the profile obtained by ref. [12] as $P(r,z) = 5.7 \times 10^{-11}$ dyn cm^{-2} $\left(\sqrt{\mathrm{r}^2 + \mathrm{z}^2}/\mathrm{kpc}\right)^{-1.5}$. The density of the jet was approximated by $\rho_j = L_j / \pi R_j^2(z) v_j \Gamma_j \left(\Gamma_j - 1\right) c^2$, where $L_j \approx$

2×10^{43} erg s^{-1} is the jet power [13], and Γ_j is the jet Lorentz factor. The jet radius R_j along the jet axis was determined by ref. [12]. Note that the pressure and density are dependent on $z_{\rm knot}$ and are different for the knots AX1A/AX1C ($z_{\rm AX1A/AX1C} \sim 292$ pc), AX2 ($z_{\rm AX2} \sim 356$ pc), and BX2 ($z_{\rm BX2} \sim 1134$ pc) [14].

The SW is characterized by the wind terminal velocity (V_∞), the mass injection rate ($\dot{M}$), and the wind temperature ($T_{\rm SW}$). In this study, we consider the knots to be a product of the interaction with power WR stars, as previously argued [6, 15]. It is assumed $V_\infty \sim 3000$ kms^{-1}, $\dot{M} \sim 10^{-4}\ M_\odot$ yr^{-1}, and $T_{\rm SW} \sim 10^6$ K [15]. The SW density and pressure are found by $\rho_{\rm SW} = \dot{M}/4\pi r^2 V_\infty$ and $P_{\rm SW} = k_B T_{\rm SW} \rho_{\rm SW}/m_H$, respectively. The SW is modelled as a constant flow, radially blown from the knot position at $z \approx z_{\rm knot}$ at simulation coordinates $r_{\rm sim} = 0$, $z_{\rm sim} = 0.5$.

2.2 Electron population and non-thermal electromagnetic spectrum

We assume that the strong and extended jet shock injects an electron energy spectrum given by power law with an exponential cutoff at a maximum energy $E_{\rm max}$. $E_{\rm max}$ is calculated by equalizing the acceleration and energy-loss timescales. The acceleration timescale is estimated as $\eta D_B/c^2\beta^2_{\rm ahead}\cos^2\theta$, where D_B is the Bohm diffusion coefficient, $\beta_{\rm ahead}$ is the speed ahead the shock, and $\eta \geq 1$ accounts for deviations from the idealized regime of Bohm diffusion. The factor $\cos^2\theta$ is an approximate way to account for the likely dropping in the acceleration efficiency with the shock obliquity and the effects of the velocity projection.

Synchrotron and Inverse Compton energy losses are assumed to be the main processes causing the cooling of electrons around the knots. The strength of the magnetic field in each cell is estimated from the thermal pressure by $B = \sqrt{\beta_m} B_P = \sqrt{8\pi P \beta_m}$, where P is the local thermal pressure measured in dyn cm^{-2}. The range of values for β_m is estimated based on constraints for the magnetic field for the knots ($40 - 80\ \mu$G [2, 9]), as $\beta_m^{\rm AX1} \sim 200 - 810$, $\beta_m^{\rm AX2} \sim 160 - 670$, and $\beta_m^{\rm BX2} \sim 50 - 210$. The local radiation density is obtained by fitting the expression $U_{\rm rad}(z) = U_0 z^n$ around the position of each knot, where $U_{\rm rad}$ considers contributions from the galactic core, starlight, and dust lane. The core and starlight components are taken from [8]. The contribution from the kpc-scale dust lane found around the galaxy is approximated as a 30 K blackbody with luminosity $L_{\rm dust} \approx 10^{44}$ erg s^{-1}, whose energy density is taken as a constant in the spatial scale of the knots, such that the energy density is $\sim L_{\rm dust}/4\pi R^2_{\rm dust} c$.

In these circumstances, $E_{\rm max}$ is estimated as

$$\frac{E_{\rm max}}{\rm GeV} = \frac{\chi}{\beta_m^{1/4}} \frac{\beta_{\rm jet}}{G(z_{\rm shock})^{1/2}} \left(\frac{B_P}{\frac{B_P^2}{\beta_m}(t_{\rm acc}/t_{\rm sync}) + U_{\rm rad}(t_{\rm acc}/t_{\rm IC})} \right)^{1/2}, \quad (1)$$

where $\beta_{\rm jet}$ is the jet speed ahead the shock in speed of light units, $t_{\rm sync} = 1.25 \times 10^{10}$ yr, $t_{\rm IC} = 5.0 \times 10^{-4}$ yr, and $t_{\rm acc} = 1.17 \times 10^{-6}$ yr. $\chi \equiv \eta^{-1/2}$ is a free parameter that accounts for limitations on the acceleration efficiency. Factor $G(z_{\rm shock}) = 1 + (2ar)^2$ provides the correction for shock obliquity. The geometry of the jet shock can be described by a parabola, $z_{\rm shock} = ar^2 + b$, where a and b are obtained by fitting the shock profile from the RHD simulations ($a_{\rm AX1} = 3.658$, $a_{\rm AX2} = 3.588$, and $a_{\rm BX2} = 3.914$).

After being injected by the shocks, electrons with energy above a critical energy E_b will suffer the effects of cooling, resulting in a broken power law energy spectrum. Assuming a constant

injection from the shocks, the system reaches a stationary state, such that E_b depends only on the position on the simulation grid. The energy spectrum at each cell (i, j) is written as

$$\left.\frac{dN}{dE}\right|_{i,j} = A_{i,j} e^{-E/E_{\max,\mathrm{ij}}} \begin{cases} (E/E_0)^{-p}, & E < E_{b,ij} \\ (E_{b,ij}/E_0)^{-1}(E/E_{b,ij})^{-(p+1)}, & E > E_{b,ij} \end{cases}. \quad (2)$$

Assuming the energy deposited in non-thermal proportional to the thermal energy of the cells, we estimate $A_{ij} = A_0 P_{ij} V_{ij}$, where $V_{ij} = 2\pi r \delta r \delta z$ is the volume of the cell, and A_0 a normalization constant. A_0 and the spectral index p are obtained from the radio and X-ray data available for each knot. E_b is obtained from the temporal cooling from $E_{\max}$, evolved with the fluid in the RHD simulation as a passive scalar $Q = \rho^{1/3}/E_b$ in a generalization of the method described in ref. [16].

The spectral energy distribution (SED) from the electron population is evaluated using the `NAIMA` library [17].

3. Knots AX1, AX2 and BX2

To test the hypothesis of the jet/SW collision as the origin of the knots, a detailed analysis of the model for the knots AX1A/AX1C, AX2, and BX2 was made. The value of p was obtained assuming a synchrotron origin for radio and X-ray emission from the knots. In this case, $p = 2\alpha + 1$, where α is the radio to X-ray spectral index. Based on the data of ref. [8], $p_{\mathrm{AX1A}} = 2.40$, $p_{\mathrm{AX1C}} = 2.43$ [1], $p_{\mathrm{AX2}} = 2.66$, and $p_{\mathrm{BX2}} = 2.27$. Two values for the acceleration efficiency χ (0.01 and 1) were explored. The normalization constant A_0 was chosen to normalize the curves to the upper and lower uncertainties of *Chandra* X-ray data at 1 keV for $\chi = 1$ and $\chi = 0.01$, respectively.

To compare the simulation results to the data, we define the emission of the knot centroid. The knot centroid radius was defined as half the *Chandra* resolution ($\sim$ 9 pc at the distance of Cen A) for knots AX1A, AX1C, and AX2, whose sizes are 2.6, 5.5, and 8.8, respectively [8]. BX2 presents a size 11.3 pc [8], and then the centroid of the knot BX2 was defined as half the knot radius. The total centroid emission was obtained by summing the non-thermal emission from cells within the centroid region. Figure 1 shows the SED obtained for the knots' centroids. For knots AX2 and BX2, the radio and X-ray measurements are satisfactorily reproduced in all scenarios considered. This constrains the maximum energy for electrons to $\gtrsim$ 40 TeV. The drop in the X-ray flux for knots AX1A/AX1C requires a significantly reduced maximum energy. An approximate match was found for $\chi = 0.002$, indicating $E_{\max} \lesssim 6$ TeV.

The validity of the model was further verified by comparing the size of the knots (σ) obtained from the X-ray signal from our model with the *Chandra* measurements. A synthetic X-ray image was built by summing the emissivity between $[0.9, 2.0]$ keV of each cell, perpendicular to the jet axis. For a fair comparison with the *Chandra* images, a Gaussian filter is used with a standard deviation of 0.5 arcsec. The knot size was calculated according to refs.[8, 14]. We obtained $\sigma_{\mathrm{AX1}} = 6.9$ pc, $\sigma_{\mathrm{AX2}} = 9.2$ pc, independent of χ, and $\sigma_{\mathrm{BX2}} = 11.8 - 13$ pc for $\chi = 0.01 - 1$. Comparing these values to the obtained in ref. [8], the sizes found by the model are larger by factors $\sim$ 150 %, 25 %, 5 %, 4 – 15 %, for AX1A, AX1C, AX2, and BX2, respectively. This indicates that the model is a suitable approximation for knots AX1C, AX2, and BX2, but not for knot

[1] For knots AX1A and AX1C, p was estimated using the VLA radio data and the first point of *Chandra* X-ray data.

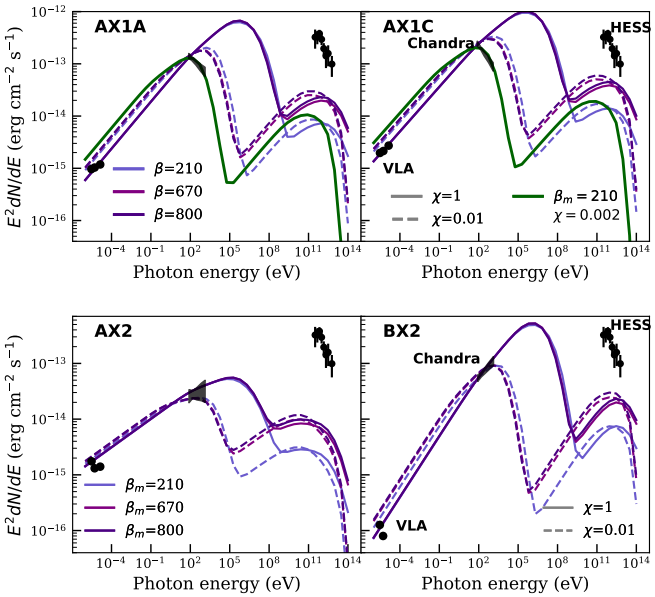

Figure 1: SED for AX1A, AX1C, AX2 and BX2 knots centroid. The circles and butterfly regions show the measurements of VLA, *Chandra*, and HESS. The different colours represent different values for β_m, and the solid and dashed lines denote $\chi = 1$ and $\chi = 0.01$, respectively. For knots AX1A and AX1C, the additional SED for $\chi = 0.002$ is also plotted. Reproduced from de Oliveira et al. [10] licensed under CC BY 4.0.

AX1A. AX1A (A1A) requires an alternative hypothesis for its origin. Figure 2 presents the X-ray morphology obtained for the knot BX2 for $\chi = 0.01$ and $\chi = 1$ (similar profiles were obtained for the other knots). The qualitative profile obtained from the simulation is compatible with the X-ray images of the knots (compare with ref. [2]). The knot centroid produces a stronger signal, but an extended X-ray tail is also visible. The emission is dependent on the maximum energy achievable, since a lower maximum energy implies a flux suppression at the end of the considered X-ray range, resulting in a lower integrated number of photons.

4. Generalization for groups of knots

Differently from VLA radio and *Chandra* X-ray measurements that can resolve the knots' emission, *Fermi*-LAT and HESS observatories provide the γ-ray emission from an area that encompasses the knots and possible diffusive emission from the jets and Inner Lobes. To verify if electrons accelerated in the knots can explain the VHE γ-ray signal, we generalize our model to include the extended tail emission and several knots. We choose stationary X-ray knots from groups AX (AX2, AX4A, AX5, and AX6) and BX (BX1, BX2, and BX4) according to ref. [5]. The RHD simulation for knot AX2 and BX2 will be used as a model for the knots in the AX- and BX-groups, respectively. The parameters p and A_0 will be chosen according to the data available for each knot analyzed. For each knot, A_0 will be corrected by $f_i = j_{X,\,i}/j_{X,\,\mathrm{AX2}}$ for AX2-like knots and $f_i = j_{X,i}/j_{X,\,\mathrm{BX2}}$ for BX2-like knots, where j_X is the X-ray flux density at 1 keV,. The electron

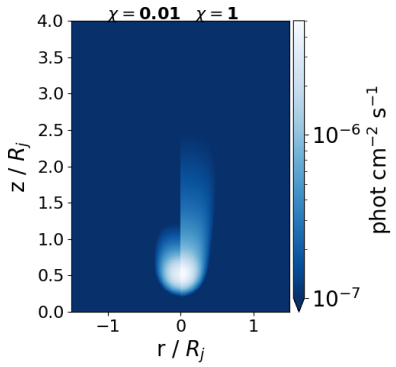

Figure 2: Synthetic X-ray image for the model of knot BX2 with $\beta_m = 210$ for $\chi = 0.01$ (left) and $\chi = 1$ (right). Colours are shown on a logarithmic scale, truncated at 10^{-7} photons cm^{-2} s^{-1}. The theoretical predictions have been smoothed using a 3 pixel rms Gaussian to compare with ref. [2]. Reproduced from de Oliveira et al. [10] licensed under CC BY 4.0.

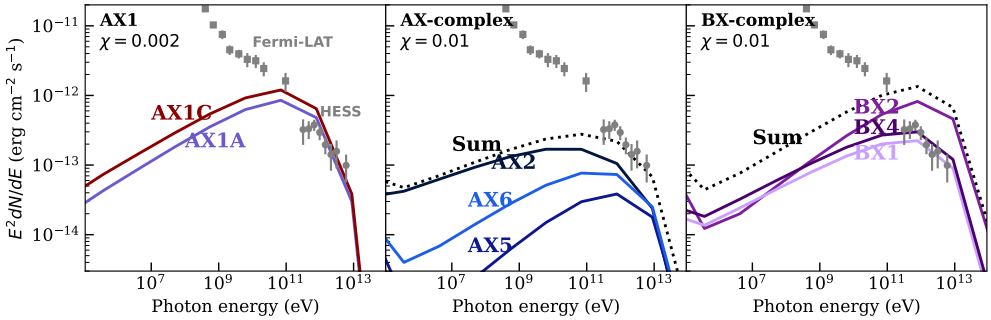

Figure 3: Total non-thermal emission predicted for different knot groups for $\beta_m = 210$, with $\chi = 0.01$ for AX- (centre) and BX-complex (right), and $\chi = 2 \times 10^{-3}$ for AX1A/AX1C (left). Reproduced from de Oliveira et al. [10] licensed under CC BY 4.0.

spectral index is taken as $p = 2\alpha^X_{4.8} + 1$, based on the radio to X-ray data available in ref. [3] [2].

Figure 3 shows the SED obtained for the γ-ray energy range for $\beta_m = 210$ and $\chi = 0.01$. The brighter γ-ray sources in the jet are AX1A, AX1C, and BX2. Due to the higher maximum energy, BX2 contributes with high-energy γ rays than the AX1 knots. The total AX-complex emission agrees with the HESS measurements, while the γ-ray emission from the BX-complex overcomes that from the AX-complex, and exceeds the γ-ray flux measured by HESS.

5. Knots as UHECR accelerators ?

Being suitable sites for electrons accelerations up to relativistic energies, we test whether knots could produce ultra-high-energy cosmic rays (UHECR). Assuming the acceleration occurs at the shock wave that defines the knot centroid, we estimate a Hillas energy $E_{\rm Hillas} \sim Z \times$

[2] Knots AX4A and BX1 were not detected in radio, and their spectral index was taken equal to that from AX6 and BX4, respectively, based on the similarities between their spectral index in the X-ray range.

10^{-4} EeV(B/μG)(R/pc). Taking the upper limit $B \sim 80$ μG, we estimate $E^{AX1}_{\rm Hillas} \sim 0.2Z$, $E^{AX2}_{\rm Hillas} \sim 0.2Z$, $E^{BX2}_{\rm Hillas} \sim 0.4Z$ EeV. This maximum energy represents the optimistic scenario in which the diffusion regime at the acceleration site follows Bohm diffusion. In this way, knots seem to be unable to explain nuclei with energies $\sim 10-100$ EeV observed. Despite that, knots can be suitable places to provide heavier elements, not usually expected to constitute the jet, and necessary to explain the UHECR composition, as previously proposed [18, 19].

6. Conclusion

We tested the hypothesis of knots as particle accelerators responsible for the VHE γ radiation detected in Cen A. By studying the brighter knots AX1A, AX1C, AX2, and BX2, we showed that the jet/SW model provides a satisfactory explanation for the origin of stationary knots. The shock produced by the collision can provide a plausible explanation for the X-ray and radio knots, as well as the VHE γ-ray energy emission observed from the Cen A jet. By combining the centroid and extended region of the knots from AX and BX groups is possible to explain the γ-ray signal measured by HESS. In a future publication, we will explore the potential of CTAO to study particle acceleration from knots in Cen A.

Acknowledgments

The authors acknowledge the National Laboratory for Scientific Computing (LNCC/MCTI, Brazil) for providing HPC resources of the SDumont supercomputer (http://sdumont.lncc.br) and the University of Oxford Advanced Research Computing (ARC) facility (http://dx.doi.org/10.5281/zenodo.22558). This study was financed, in part, by the Sao Process Number 2025/03325-5, 2023/16753-0, 2021/01089-1, 2020/15453-4, and 2019/10151-2. JHM acknowledges funding from a Royal Society University Research Fellowship (URF\R1\221062).

References

[1] G.L. Harris, M. Rejkuba and W.E. Harris, *The distance to NGC 5128 (Centaurus A)*, *Publications of the Astronomical Society of Australia* **27** (2010) 457.

[2] B. Snios, S. Wykes, P.E.J. Nulsen, R.P. Kraft, E.T. Meyer, M. Birkinshaw et al., *Variability and Proper Motion of X-Ray Knots in the Jet of Centaurus A*, *The Astrophysical Journal* **871** (2019) 248.

[3] J.L. Goodger, M.J. Hardcastle, J.H. Croston, R.P. Kraft, M. Birkinshaw, D.A. Evans et al., *Long-term monitoring of the dynamics and particle acceleration of knots in the jet of Centaurus A*, *The Astrophysical Journal* **708** (2009) 675.

[4] The H.E.S.S. Collaboration, *Resolving acceleration to very high energies along the jet of Centaurus A*, *Nature* **582** (2020) 356.

[5] D. Bogensberger, J.M. Miller, R. Mushotzky, W.N. Brandt, E. Kammoun, A. Zoghbi et al., *Superluminal proper motion in the X-ray jet of Centaurus A*, *The Astrophysical Journal* **974** (2024) 307.

[6] M.J. Hardcastle, D.M. Worrall, R.P. Kraft, W.R. Forman, C. Jones and S.S. Murray, *Radio and X-Ray observations of the jet in Centaurus A*, *The Astrophysical Journal* **593** (2003) 169.

[7] W. Bednarek and R.J. Protheroe, *Gamma-rays from interactions of stars with active galactic nucleus jets*, *Monthly Notices of the Royal Astronomical Society* **287** (1997) L9.

[8] K. Tanada, J. Kataoka and Y. Inoue, *Inverse Compton Scattering of Starlight in the kiloparsec-scale jet in Centaurus A: The origin of excess TeV γ-ray emission*, *The Astrophysical Journal* **878** (2019) 139.

[9] T. Sudoh, D. Khangulyan and Y. Inoue, *Physical conditions and particle acceleration in the kiloparsec jet of Centaurus A*, *The Astrophysical Journal Letters* **901** (2020) L27.

[10] C. de Oliveira, J.H. Matthews and V. de Souza, *The origin of the very-high-energy radiation along the jet of Centaurus A*, *Monthly Notices of the Royal Astronomical Society* **539** (2025) 3697.

[11] A. Mignone, G. Bodo, S. Massaglia, T. Matsakos, O. Tesileanu, C. Zanni et al., *PLUTO: A numerical code for computational astrophysics*, *The Astrophysical Journal Supplement Series* **170** (2007) 228.

[12] S. Wykes, B.T. Snios, P.E.J. Nulsen, R.P. Kraft, M. Birkinshaw, M.J. Hardcastle et al., *A 1D fluid model of the Centaurus A jet*, *Monthly Notices of the Royal Astronomical Society* **485** (2019) 872.

[13] S.G. Neff, J.A. Eilek and F.N. Owen, *The complex north transition region of Centaurus A: A galactic wind*, *The Astrophysical Journal* **802** (2015) 88.

[14] R.P. Kraft, W.R. Forman, C. Jones, S.S. Murray, M.J. Hardcastle and D.M. Worrall, *Chandra observations of the x-ray jet in centaurus a*, *The Astrophysical Journal* **569** (2002) 54.

[15] A.L. Müller and A. Araudo, *Cosmic ray acceleration by multiple shocks in the jets of active galactic nuclei*, *EPJ Web Conf.* **283** (2023) 04005.

[16] E.H. Ayache, H.J. van Eerten and R.W. Eardley, *gamma: a new method for modelling relativistic hydrodynamics and non-thermal emission on a moving mesh*, *Monthly Notices of the Royal Astronomical Society* **510** (2021) 1315.

[17] V. Zabalza, *naima: a Python package for inference of relativistic particle energy distributions from observed nonthermal spectra*, *Proc. of International Cosmic Ray Conference 2015* (2015) 922 [1509.03319].

[18] A.L. Müller and A. Araudo, *Active Galactic Nuclei Metallicity Enrichment and UHECR Composition*, *PoS* **UHECR2024** (2025) 105.

[19] S. Wykes, A.M. Taylor, J.D. Bray, M.J. Hardcastle and M. Hillas, *UHECR propagation from Centaurus A*, *Nuclear and Particle Physics Proceedings* **297-299** (2018) 234.